Quantifying the Importance of Micellar Microstructure and Electrostatic Interactions on the Shear-Induced Structural Transition of Cylindrical Micelles

M. T. Truong and L. M. Walker*

Department of Chemical Engineering, Center for Complex Fluids Engineering, Carnegie Mellon University, Pittsburgh, Pennsylvania 15213

Received August 23, 2001. In Final Form: December 6, 2001

Using static light scattering (SLS) and small-angle neutron scattering (SANS) in conjunction with rheological measurements, the significance of electrostatic interactions and micellar microstructure to the formation of shear-induced structures (SIS) in systems of dilute aqueous cylindrical micelles is investigated. This is accomplished through a systematic study of the influence of increasing NaCl concentration on the dilute aqueous micellar system of 11 mM cetyltrimethylammonium *p*-toluenesulfonate (CTAT). Concurrent with increases in the zero-shear viscosity (η_o), low NaCl concentrations lead to the growth of micelles through increases in the degree of screening of electrostatic interactions. These systems, which exhibit discernible electrostatic or correlation peaks in the SANS results, undergo shear-induced structural transitions, whereby critical shear rates tend to increase with NaCl concentration. With further increases in the NaCl concentration, intermicellar electrostatic interactions are adequately screened, and no SIS is observed. The addition of NaCl to these systems increases the micellar flexibility, as shown by SLS. The η_o of these systems decreases, and the critical shear rates for these shear-thinning systems increases, consistent with expectations for dilute polyelectrolyte systems.

Introduction

In rheological measurements, dilute cationic surfactant systems exhibit an apparent shear-thickening behavior. In addition to rheological measurements,[1−3] shear small-angle neutron scattering (SANS),[4−7] light scattering microscopy,[8,9] birefringence,[3,10,11] and cryo-TEM[8,11,12] techniques have been used to study the structure formed under shear. These abrupt increases in viscosity occur at shear rates much lower than those expected for inertial flow instabilities. Thebaud verified that the shear-induced structure (SIS) of cetyltrimethylammonium *p*-toluenesulfonate (CTAT) is not a flow instability due to curved streamlines by verifying the apparent thickening in Poiseuille flow.[13] This was accomplished using shear SANS studies, where the SIS is shown by dramatic scattering anisotropy, indicating structural alignment in the direction of the flow. Although many investigations of SIS involved different surfactant systems, the general requirement for this transition appears to be that the micellar system form charged, rodlike (cylindrical) micelles in dilute solution.

Various qualitative models have been proposed that attempt to explain the microscopic changes that occur during this transition. For example, Rehage et al. proposed a model in which large micelles are formed when small micelles collide in shear flow and fuse together.[10] Hu et al. found evidence of a secondary, more viscous phase, which grew from the moving wall in a concentric cylindrical geometry, indicative of a flow-induced phase transition.[14] Berret et al. suggested a shear-induced transition from rodlike to longer, more flexible entangled structures.[7] Recently, Barentin and Liu proposed that the SIS arises through the formation of micellar bundles, resulting from counterion-assisted intermicellar attraction.[15] Although the exact nature of the transition is somewhat controversial, it is well-established that this phenomenon is very sensitive to changes in the micelles and their environment.[7,13] Our previous work with nonionic polymers indicates that subtle changes in the structure of an added polymer can be used to control SIS formation.[16] As the structure of the micelles changes with solution conditions, the magnitude of the critical shear rate is sensitive to external parameters. As such, the transition itself is susceptible to subtle changes in the micellar structure.

The objective of this work is to quantify the importance of micellar microstructure on macroscopic behavior. More specifically, changes in micellar length and flexibility, as well as intermicellar electrostatic interactions, are investigated through systematic structural and rheological studies of 11 mM cetyltrimethylammonium *p*-toluenesulfonate (CTAT) in D_2O with added salt ranging from 0 to 200 mM sodium chloride (NaCl). The only anionic species are the organic counterion *p*-toluenesulfonate (or

* Corresponding author (lwalker@andrew.cmu.edu)

(1) Gravsholt, S. *Proc. Int. Congr. Rheol.* **1980**, *8*, 629.
(2) Rehage, H.; Hoffmann, H. *Rheol. Acta* **1982**, *21*, 561.
(3) Hu, Y.; Wang, S.; Jamieson, A. J. *Rheol.* **1993**, *37*, 531.
(4) Hoffmann, H.; Hofmann, S.; Rauscher, A.; Kalus, J. *Prog. Colloid Polym. Sci.* **1991**, *84*, 24.
(5) Jindal, V. K.; Kalus, J.; Pilsl, H.; Hoffmann, H.; Lindner, P. *J. Phys. Chem.* **1990**, *94*, 3129.
(6) Schmitt, V.; Schosseler, F.; Lequeux, F. *Europhys. Lett.* **1995**, *30*, 31.
(7) Berret, J.-F.; Gamez-Corrales, R.; Oberdisse, J.; Walker, L. M.; Lindner, P. *Europhys. Lett.* **1998**, *41*, 677−682.
(8) Lu, B.; Li, X.; Scriven, L.; Davis, H.; Talmon, Y.; Zakin, J. *Langmuir* **1998**, *14*, 8.
(9) Boltenhagen, P.; Hu, Y.; Matthys, E. F.; Pine, D. J. *Europhys. Lett.* **1997**, *38*, 389.
(10) Rehage, H.; Wunderlich, I.; Hoffmann, H. *Prog. Colloid Polym. Sci.* **1986**, *72*, 51.
(11) Oda, R.; Panizza, P.; Schmutz, M.; Lequeux, F. *Langmuir* **1997**, *13*, 6407.
(12) Keller, S.; Boltenhagen, P.; Pine, D.; Zasadzinski, J. *Phys. Rev. Lett.* **1998**, *80*, 2725.
(13) Thebaud, B. An Examination of Shear-Induced Micellar Structures in Tube Flow Using Small Angle Neutron Scattering. Ph. D. Thesis, Carnegie Mellon University, Pittsburgh, PA, 1998.
(14) Hu, Y. T.; Boltenhagen, P.; Pine, D. J. *J. Rheol.* **1998**, *42*, 1185.
(15) Barentin, C.; Liu, A. J. *Europhys. Lett.* **2001**, *55*, 432−438.
(16) Truong, M. T.; Walker, L. M. *Langmuir* **2000**, *16*, 7991−7998.

10.1021/la015551x CCC: $22.00
Published on Web 01/29/2002

tosylate) and smaller chloride ions. Rheological measurements are used to quantify the critical shear rate for the SIS transition, and shear SANS is used to verify the extent of structural alignment. Static SANS and static light scattering (SLS) measurements are used to evaluate the effects of NaCl on the quiescent structure of the micelles. A combination of existing models is used to extract information about micellar microstructure from scattering.

2. Experimental Section

2.1. Materials. Cetyltrimethylammonium *p*-toluenesulfonate (CTAT) was used as received from Sigma Chemical Co. The purity of CTAT was verified using surface tension measurements [no depression was observed near the critical micelle concentration (cmc)]. Sodium chloride (NaCl) was used as received from Fisher Scientific. Deuterium oxide (D_2O) from Aldrich Chemical Co., with a reported atom fraction of 99.9% deuterium, refractive index (n) of 1.328, and density of 1.107 g/cm^3, was used as the solvent in all experiments. Mixed NaCl and CTAT samples were prepared by mixing appropriate volumes of stock solutions of CTAT/D_2O, CTAT/NaCl/D_2O, and D_2O. Samples were shaken manually and placed in a 30 °C oven for at least 6 h. One hour prior to use, the samples were placed in a 25 °C bath. All rheological and structural studies were performed at 25 °C using 11 mM CTAT in D_2O with varying NaCl concentrations.

2.2. Methods. Rheological studies were performed on a Rheometric Scientific ARES strain-controlled rheometer. Because of the wide range of measured viscosities, two geometries were used. The first geometry is cone and plate, with both fixtures made of titanium. The cone has a diameter of 25 mm, an angle of 0.0402 rad, and an operating gap of 0.048 mm. The plate is 50 mm in diameter and its temperature is controlled to within ±0.1 °C using a circulating fluid bath. The second geometry is Couette or concentric cylinders, with both cylinders made of stainless steel. The outer cylinder is temperature-controlled and is 34 mm in diameter. The inner cylinder is 32 mm in diameter, yielding a gap of 1.0 mm. A humidity cover was used to minimize sample evaporation during testing. Strain sweep experiments were performed, and the steady stress was determined to within 2% deviation. The reported viscosity is the ratio of the steady measured stress to the applied shear rate. Additional transient tests were done at various shear rates to verify that steady-state values were reached.

Small-angle light scattering (SLS) studies were performed with a Brookhaven Instruments Corporation BI-200SM goniometer. With a green diode laser light source with a wavelength of 532 nm and an angular range of $45° \le \theta \le 135°$, the scattering vector range was $0.0012 \le q \le 0.0029$ Å^{-1}. Decalin ($n = 1.474$) was used as a refractive index matching fluid, surrounding the sample cuvette. After subtraction of the scattering from D_2O, the scattered intensities were normalized using toluene as the reference. The values used for the Rayleigh scattering ratio (R) and refractive index of toluene were 0.003 96 m^{-1} and 1.5, respectively.

Small-angle neutron scattering (SANS) experiments were performed at the NIST facility in Gaithersburg, MD, on the 30-m SANS-NG3 beamline. At a neutron wavelength of 6 Å with a spread of 0.147 Å and at detector distances of 3 and 12 m with a 20-cm detector offset, a q range of 0.004−0.178 Å^{-1} was obtained. For experiments under shear, samples were placed in a quartz Couette shear cell with a gap of 0.5 mm, an outer rotating cylinder of radius 29.5 mm, and a stationary inner cylinder. Samples examined only at rest were placed in 1-mm-thick sample cells with quartz windows. Both sample holders were temperature-controlled to within ±0.1 °C using a circulating fluid bath and were designed by NIST. All SANS data were corrected for empty cell scattering and detector background and sensitivity using standard techniques.[17] The scattered intensities were then converted to absolute intensities using calibrated standards provided by NIST. For CTAT, the coherent scattering length (b_m) is 1.92×10^{-12} cm, based on a molecular structure of $C_{16}H_{33}N(CH_3)_3SO_3C_6H_4CH_3$. Previous work by Bartet et al. on the binding affinities of *p*-toluenesulfonate (Tos^-) and chloride (Cl^-) ions showed that close to 95% of the Cl^- ions remain unbound to the CTA^+ micelles.[18] Therefore, the addition of NaCl to the micellar system was considered in the calculation of the scattering length density of the solvent (ρ_s). ρ_s was calculated using the composition of NaCl by weight, assuming that NaCl has no effect on the density of D_2O. Consequently, the scattering contrast ($\Delta\rho$) varies from 6.13×10^{10} cm^{-2} for CTAT with no NaCl in D_2O to 6.10×10^{10} cm^{-2} for CTAT at the highest NaCl concentration in D_2O.

(17) NIST Center for Neutron Research, Gaithersburg, MD.

3. Theoretical Background

In the analysis of scattering results, two approaches were used. The first was to model for local micellar structure using SANS data for $0.05 \le q \le 0.08$ Å^{-1}. The reason for this intermediate q range is explained below. The second approach was to use data from both SANS and SLS. For this extended q range, the overall micellar length, polydispersity (in length) and degree of flexibility were determined. In addition to these two methods, rheological results were used to estimate micellar lengths for systems that formed shear-induced structures (SIS).

3.1. Analysis of Intermediate-*q* Scattering. At intermediate q values, the Guinier approximation was used to extract information about the micellar microstructure[19]

$$qI(q) = K_{BR} \exp\left(\frac{-q^2 R_{g,cs}{}^2}{2}\right) \quad (1)$$

where q is the scattering vector, $I(q)$ is the absolute scattered intensity, and $R_{g,cs}$ is the radius of gyration of the micellar cross section. K_{BR} is the bending rod constant, defined as

$$K_{BR} = \pi c \left\langle \frac{N}{L} \right\rangle_w (b_m - V_m \rho_s)^2 \quad (2)$$

where c is the surfactant concentration; $\langle N/L \rangle_w$ is the weight-average number of surfactant monomers per unit length; b_m and V_m are the coherent scattering length and unit volume of the surfactant monomer, respectively; and ρ_s is the scattering length density of the solvent. $R_{g,cs}$ and K_{BR} can be calculated from a simple linear fit of a bending rod or Holtzer plot.[20,21] For all of the data presented, this linear behavior occurred over a q range of 0.04−0.08 Å^{-1}. For a circular cross section, the radius (r_{cs}) is given by $\sqrt{2}R_{g,cs}$. For a cylindrical micelle, V_m is equal to $A_{hg}r_{cs}$, where A_{hg}, the micellar surface area per surfactant headgroup, is $2\pi r_{cs}2(L/N)$. Here, it is assumed that $N/L = \langle N/L \rangle_w$. This method was used to calculate r_{cs} and A_{hg}.

3.2. Analysis of Full Range of Scattered Intensity. Three models were used to analyze the full static scattering curves. The first is that for uniform rigid cylinders as formalized by Hayter and Penfold.[22] The next two models were developed by Pedersen and Schurtenberger,[23] which use a discrete representation of Kratky and Porod's wormlike chain model to perform Monte Carlo simulations on semiflexible cylinders with and without excluded-volume interactions. There are many variations of this model. The methods used in this work for flexible cylinders of monodisperse and polydisperse lengths with excluded-volume effects are briefly outlined below. All of the models

(18) Bartet, D.; Gamboa, C.; Sepulveda, L. *J. Phys. Chem.* **1980**, *84*, 274.
(19) Magid, L.; Han, Z.; Li, Z. *Langmuir* **2000**, *16*, 149−156.
(20) Casassa, E. F. *J. Chem. Phys.* **1955**, *23*, 596−597.
(21) Holtzer, A. *J. Polym. Sci* **1955**, *17*, 432−434.
(22) Hayter, J. B.; Penfold, J. *J. Phys. Chem.* **1984**, *88*, 4589.
(23) Pedersen, J. S.; Schurtenberger, P. *Macromolecules* **1996**, *29*, 7602.

used in this work assume no interactions between the micelles, i.e., no structure-factor effects. As will be shown, this can lead to limitations in the applicability of the models. In fitting these models to the data, $I(q)$ had the general form

$$I(q)_{\text{predicted}} = (\text{scale})\langle P(q)\rangle + \text{bkgd} \tag{3}$$

where "scale" includes scattering length density contrast between solvent and micelle and concentration of micelles and "bkgd" is the scattering from the background and/or solvent. $\langle P(q)\rangle$ is the average form factor as calculated by any of the three models presented below depending on whether micellar flexibility and polydispersity in micellar length are considered. To ascertain the goodness of fit, the accuracy of the predicted intensities [$I(q)_{\text{predicted}}$] was quantified by calculating residuals as a function of q

$$\text{residual}(q) = \frac{I(q)_{\text{predicted}} - I(q)}{I(q)_{\text{predicted}}} \tag{4}$$

a. Uniform Rigid Cylinders. The form factor for a system of uniform noninteracting rigid rods of length L and cross-sectional radius R is given by

$$P(q) = \frac{\text{scale}}{V_{\text{cyl}}}\int_0^{\pi/2} f(q,\alpha)\sin\theta\, d\alpha \tag{5}$$

where V_{cyl}, the volume of the cylinder, is $\pi R^2 L$ and α is the angle between the cylinder axis and the scattering vector q. The single-particle form factor, $f(q,\alpha)$, is given by[22]

$$f(q,\alpha) = 2(\Delta\rho)V_{\text{cyl}}\, j_o\left(\frac{qL}{2}\cos\alpha\right)\frac{J_1(qR\sin\alpha)}{qR\sin\alpha} \tag{6}$$

where $\Delta\rho$ is the scattering length density contrast between solvent and micelle, $j_o(x)$ is $\sin(x)/x$, and $J_1(x)$ is the first-order Bessel function of x. As will be demonstrated, R is determined by the method outlined in the previous section, and the only adjustable parameter is L.

b. Uniform Flexible Cylinders. For cylinders with distinct length scales (contour length L, Kuhn length b, and cross-sectional radius R), the form factor is simply the product of contributions from the micellar cross section, $P_{\text{cs}}(q,R)$, and the wormlike chain, $P_{\text{ch}}(q,L,b)$.[24] $P_{\text{cs}}(q,R)$ is given by

$$P_{\text{cs}}(q,R) = \left[\frac{2J_1(qR)}{qR}\right]^2 \tag{7}$$

The expression for $P_{\text{ch}}(q,L,b)$ depends on the degree of chain flexibility, which is described by the quantity L/b.[23] For $L/b > 4$, Pedersen and Schurtenberger modified a calculated scattering function by Sharp and Bloomfield[25] to include excluded-volume effects. For $qb < 3.1$, $P_{\text{ch}}(q,L,b)$ incorporates the Debye function, $P_{\text{Debye}}(q,L,b)$, given by

$$P_{\text{Debye}}(q,L,b) = \frac{2[\exp(-u) + u - 1]}{u^2} \tag{8}$$

where u is $q^2R_g^2$. R_g^2 is the mean-square radius of gyration. For $qb \geq 3.1$, Pedersen and Schurtenberger created a continuous extrapolation, such that $P_{\text{ch}}(q,L,b)$ approaches the scattering function of a rod as $qb \rightarrow \infty$. For monodisperse cylinders with $L/b \leq 4$, excluded-volume effects are negligible. $P_{\text{ch}}(q,L,b)$ is simply $P_{\text{Debye}}(q,L,b)$ for $qb < q_o(L,b)$, where $q_o(L,b)$ is defined as

$$q_o(L,b) = \max\left\{\frac{a_3 b}{(R_g^2)^{1/2}}, 3\right\} \tag{9}$$

where a_3 is a constant. For $qb \geq q_o(L,b)$, $P_{\text{ch}}(q,L,b)$ is given by the same form as when $qb \geq 3.1$ for $L/b > 4$. A least-squares fitting routine was used to determine structural parameters L and b.

c. Polydisperse Flexible Cylinders. To incorporate polydispersity into the flexible cylinder model, an average $P_{\text{ch}}(q,L,b)$ was calculated using a Schulz−Zimm distribution[26,27] of lengths $N(L)$ with fixed polydispersity $M_w/M_n = 2$

$$\langle P_{\text{ch}}(q,L,b)\rangle = \frac{\int N(L)L^2 P_{\text{ch}}(q,L,b)\, dL}{\int N(L)L^2\, dL} \tag{10}$$

where $P_{\text{ch}}(q,L,b)$ is given in the previous section. R_g^2 is replaced similarly by the expression

$$\langle R_g^2\rangle^{1/2} = \left[\frac{\int N(L)L^2 R_g^2\, dL}{\int N(L)L^2\, dL}\right]^{1/2} \tag{11}$$

A least-squares fitting routine was used to determine the only two structural parameters L and b.

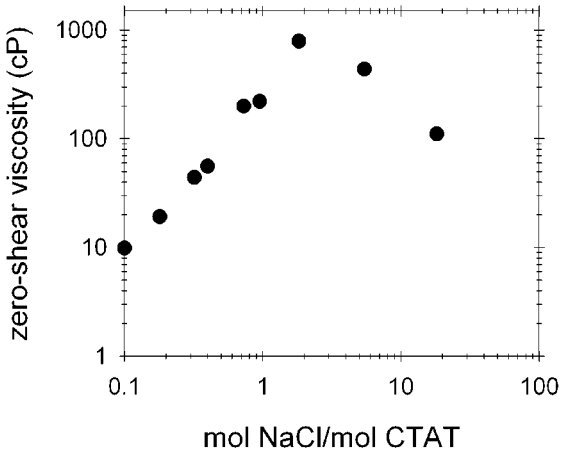

Figure 1. Effects of NaCl on the zero-shear viscosity of 11 mM CTAT in D_2O at 25 °C. In the absence of NaCl, the zero-shear viscosity is 4.4 cP.

4. Results

4.1. Rheological Studies. Rheology provides the motivation for our structural studies. To determine the structural requirements for the shear-induced structure (SIS), we characterized the onset of SIS formation as a function of composition. The addition of NaCl to 11 mM CTAT/D_2O induces dramatic rheological changes. With no added NaCl, the zero-shear viscosity (η_o) of 11 mM CTAT/D_2O is 4.4 ± 0.5 cP. At low concentrations, Figure 1 shows that NaCl can increase the η_o of the micellar system by more than two decades. A peak η_o of 793 ± 6 cP is observed at 1.8 mol of NaCl per mole of CTAT, hereafter denoted as 1.8:1. At higher NaCl concentrations, η_o decreases. The effects of NaCl on the apparent shear

(24) Pedersen, J. S.; Schurtenberger, P. *J. Appl. Crystallogr.* **1996**, *29*, 646.
(25) Sharp, P.; Bloomfield, V. A. *Biopolymers* **1968**, *6*, 1201.
(26) Schulz, G. V. *Z. Phys. Chem. B* **1939**, *43*, 25.
(27) Zimm, B. H. *J. Chem. Phys.* **1948**, *16*, 1099.

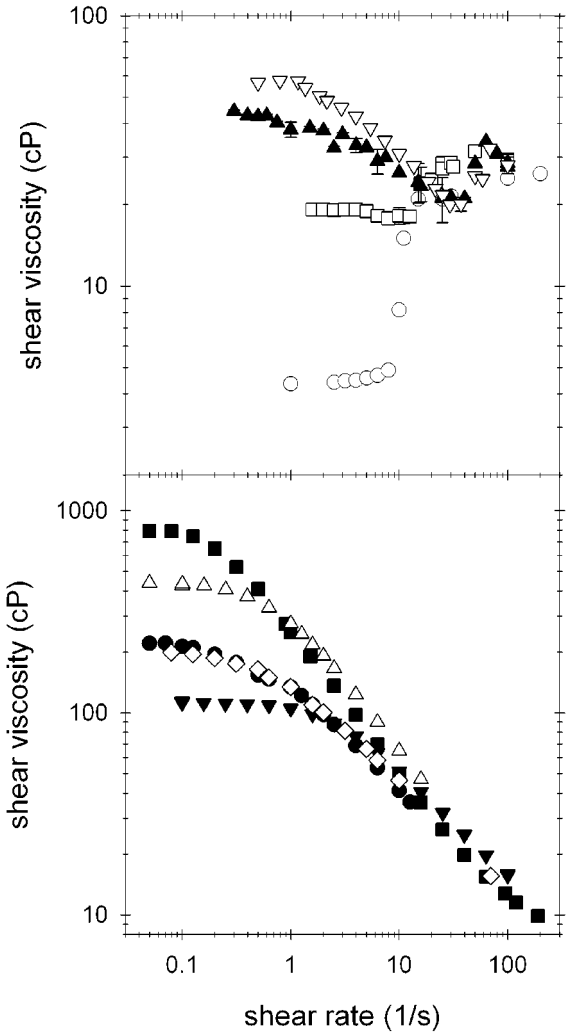

Figure 2. Effects of NaCl on the steady-state rheology of 11 mM CTAT in D_2O, reported at various molar ratios of NaCl to CTAT. The notation 2:1 refers to 2 mol of NaCl per mole of CTAT (in D_2O). In top figure (○) 0:1, (□) 0.2:1, (▲) 0.3:1, and (▽) 0.4:1. In bottom figure (◇) 0.7:1, (●) 1:1, (■) 1.8:1, (△) 5.4:1, and (▼) 18:1.

thickening of 11 mM CTAT are illustrated in Figure 2. In Figure 2a, the critical shear rate of the apparent shear thickening increases from about 10 to 15 s^{-1} as the NaCl concentration is increased from 0:1 to 0.2:1. Further increasing the concentration of NaCl to 0.3:1 and 0.4:1 leads to shear-thinning behavior at low rates and shear thickening at critical rates of 40 and 50 s^{-1}, respectively. In Figure 2b, systems with NaCl/CTAT ratios greater than 0.7:1 are shear thinning at all detectable rates. No apparent shear thickening is observed, which indicates that no shear-induced structure arises. This is verified with shear SANS, which will be discussed later. Figure 3 shows that the critical shear rates required for shear thinning exhibit a minimum at 1.8:1, the same composition at which a maximum in η_o is detected. Hence, we focus on the structural changes leading to these striking rheological changes.

4.2. Static Structural Studies. The ratio of 1.8:1 marks a change in the macroscopic flow behavior. To determine the basis of these changes, the effects of NaCl on the resting structure of 11 mM CTAT/D_2O was characterized by static light scattering (SLS) and small-angle neutron scattering (SANS). Because SANS data is on an absolute scale, we shifted the SLS data to match the low-q SANS data. This was done with the data plotted as

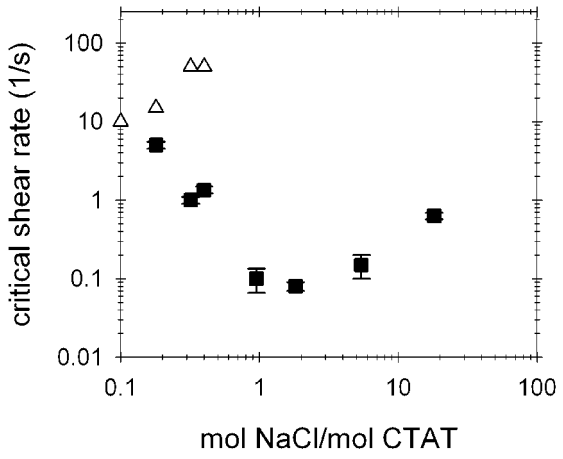

Figure 3. Effects of NaCl on the critical shear rates of shear thickening (△) and shear thinning (■) of 11 mM CTAT in D_2O.

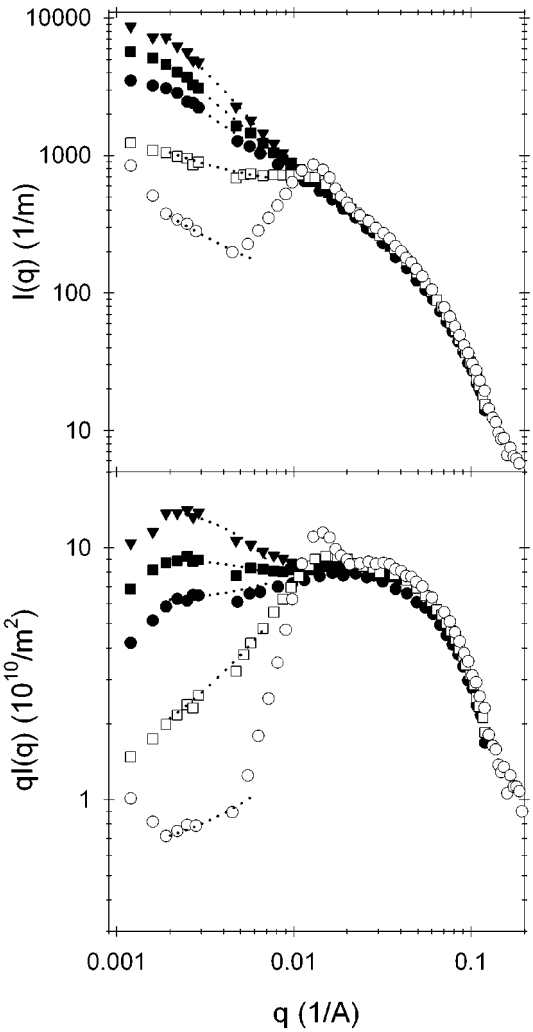

Figure 4. Effects of NaCl on the static scattering of 11 mM CTAT in D_2O. SANS ($0.0045 \leq q \leq 0.12$ Å^{-1}) and SLS ($0.0012 \leq q \leq 0.0029$ Å^{-1}) data are reported at various molar ratios of NaCl to CTAT: (○) 0:1, (□) 0.2:1, (●) 1:1, (■) 1.8:1, and (▼) 18:1.

a bending rod plot. Because both SANS and SLS data sets for 0.2:1 are linear for low-q SANS and high-q SLS, these data were used to determine the shift factor for the SLS results. The same shift factor was then used for all other systems. The absolute scattered intensities from SANS, $I(q)$, and shifted Rayleigh scattering ratios from SLS, $R(q)$, of 11 mM CTAT/D_2O with varying NaCl-to-CTAT molar

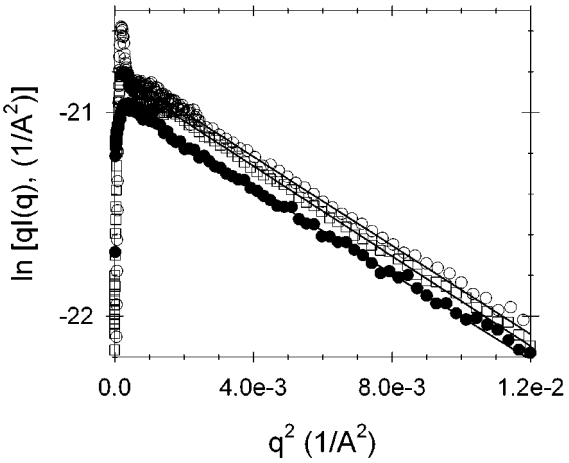

Figure 5. Linear regions of Guinier-like plots for $0.002 \leq q^2 \leq 0.006$ Å^{-2} of 11 mM CTAT in D_2O for various molar ratios of NaCl to CTAT: (○) 0:1, (□) 0.2:1, and (●) 1:1. The lines are linear fits with slopes and intercepts given in Table 1.

ratios are given simply as $I(q)$ in Figure 4a. Alternatively, these results are presented in a bending rod or Holtzer plot in Figure 4b to further examine rigid rodlike behavior. The gap between the light and neutron scattering data is filled by simply fitting a line between the two sets of data on a bending rod plot using a 5% standard deviation. These lines are shown as dotted lines in Figure 4b. Although there is a gap in q space between the SANS and SLS measurements, there is a wealth of structural information to be gained, as will be shown.

With no added NaCl, 11 mM CTAT shows a peak at 0.012 Å^{-1}. With increasing NaCl concentration, there is a gradual suppression of the magnitude of this peak and an increase in the scattered intensity as q approaches 0. At intermediate q, changes in the scattering from the micellar cross section can be analyzed using the Guinier approximation (eqs 1 and 2) to extract information about the cross-sectional radius (r_{cs}) and CTAT monomer packing density. Figure 5 demonstrates the viability of this approach with a plot of $\ln[qI(q)]$ vs q^2 for various CTAT/NaCl systems. Lines are fit to data for q^2 between 0.002 and 0.006 Å^{-2}. The lack of variation in the slope of these lines at various NaCl concentrations reflects the insensitivity of r_{cs} to NaCl. This is illustrated in Figure 6a, where calculated values for r_{cs} are shown as a function of the NaCl/CTAT ratio. Figure 6b shows that NaCl has no effect on the average area per headgroup, A_{hg}, meaning that NaCl does not significantly change the packing density of the CTAT monomers. This indicates that, although Cl^- ions might shield repulsions between neighboring CTA^+ headgroups, the local structure of the micelles is dominated by the strongly binding counterion Tos^-.[28] Local micellar structural parameters from the Guinier approximation are summarized in Table 1. Using an average number of CTAT monomers per unit micellar length (N/L) of 2 Å^{-1} and an r_{cs} value of 20 Å, the system of 11 mM CTAT in D_2O is relatively dilute, with a micellar volume fraction of 0.004. Given this low concentration of micelles, we assumed no interactions between the micelles and proceeded to model the static scattering curves. The validity of this assumption is evaluated later in this section.

In describing the structure of the micellar systems using the full range of scattered intensities, we considered the possible conformations of uniform rigid cylinders, uniform flexible cylinders, and polydisperse flexible cylinders. Scattering from mondisperse rigid cylinders is characterized by a distinct region where $I \sim q^{-n}$ with $n = 1$.[22] At higher q, n becomes 2, and the intensity decreases more dramatically as a result of scattering from the finite cross section of the cylinders. As q approaches 0, n remains smaller than 1 and greater than 0 for rigid cylinders. Scattering from flexible cylinders shares many features with that from rigid cylinders: there is a region of $n = 1$ from scattering of the persistence length (length scale of local rigidity), and n approaches 2 at higher q. At lower q, however, n is not limited to $0 < n < 1$ as in the rigid case.[23,24] From the general form of the data, we could qualitatively identity the physical conformation of a given

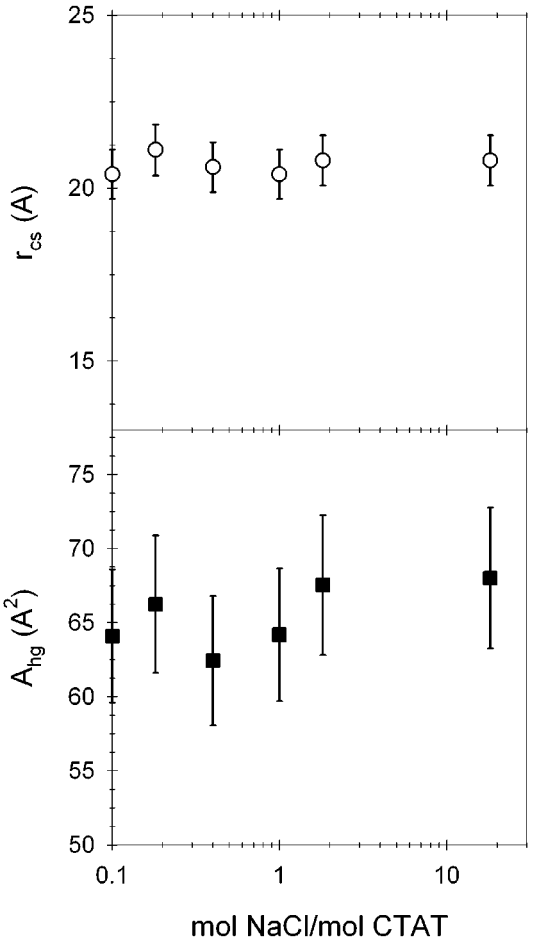

Figure 6. Structural parameters extracted using the Guinier approximation[19] at intermediate q, reported as functions of the molar ratio of NaCl to CTAT for 11 mM CTAT in D_2O: in the top figure, micellar cross-sectional radius, r_{cs}, with an error of 3.5%, and in the bottom figure, area per surfactant headgroup, A_{hg}, with an error of 7.0%. The values are summarized in Table 1.

Table 1. Effects of NaCl on the Local Micellar Structure of 11 mM CTAT/D_2O Using the Guinier Approximation[19]

mol of NaCl: mol of CTAT	slope[a]	intercept[a]	r_{cs} (Å)[b]	$(b_m - V_m\rho_s)^2$ (10^{-21} cm^2)[c]	N/L (1/Å)[d]	A_{hg} (Å^2)[e]
0:1	−107.1	−20.8	20.7	8.57	1.82	71.45
0.1:1	−103.6	−21.0	20.4	6.62	2.00	64.09
0.2:1	−110.9	−20.8	21.1	7.59	2.00	66.24
0.4:1	−106.5	−21.0	20.6	6.45	2.08	62.43
1:1	−104.1	−21.0	20.4	6.67	2.00	64.18
1.8:1	−108.6	−20.8	20.8	7.73	1.94	67.54
18:1	−108.6	−20.8	20.8	7.78	1.93	68.01

[a] From lines in Figure 5. [b] Error in r_{cs} is 3.5%. [c] b_m is 1.9×10^{-12} cm, and NaCl is taken into account in ρ_s. [d] Error in N/L is 4.0%. [e] Error in A_{hg} is 7.0%.

(28) Gamboa, C.; Rios, H.; Sepulveda, L. *J. Phys. Chem.* **1989**, *93*, 5540.

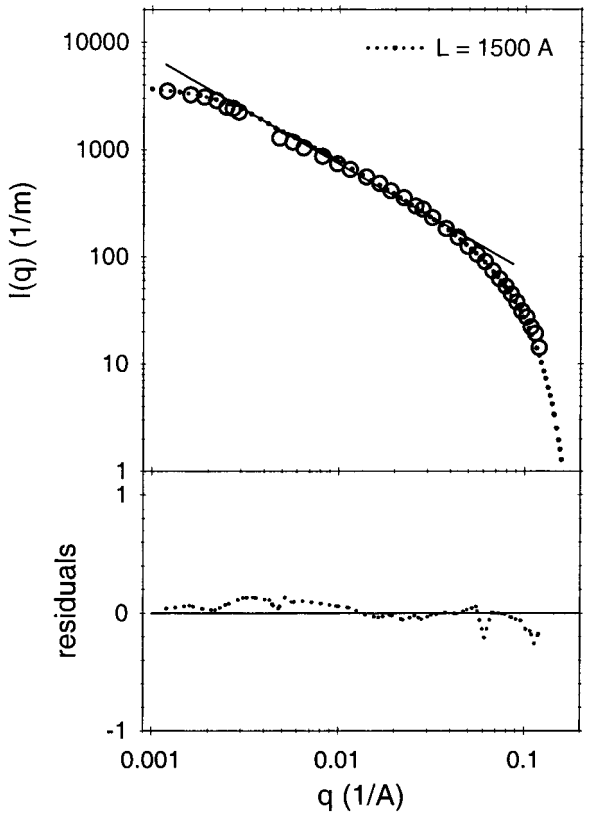

Figure 7. Comparison of the model of rigid rods[22] of 1500 Å (···) to the scattering of 11 mM CTAT/11 mM NaCl in D_2O (1:1) (○). The solid line indicates a line of slope −1. Residuals of the fit as calculated by eq 4 show slight overpredictions at low q.

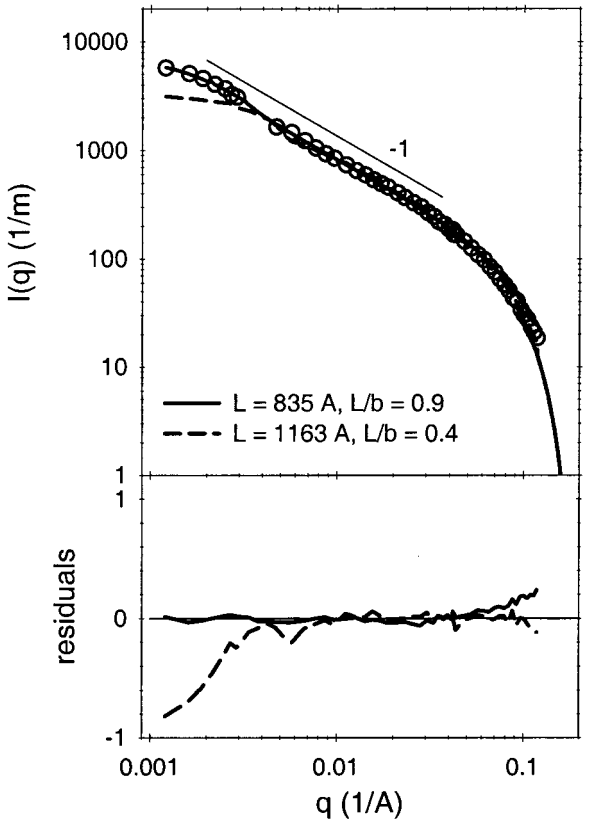

Figure 8. Comparison of various models for the scattering of 11 mM CTAT/20 mM NaCl in D_2O (1.8:1) (○). The dashed line (- - -) is the monodisperse flexible cylinder model,[23] and the thick solid line (—) is the polydisperse, flexible cylinder model.[23] The best overall fit is given by polydisperse flexible cylinders.

system, i.e., if micellar flexibility is apparent. Building on this qualitative structural interpretation, the appropriate model was chosen solely to extract quantitative parameters. Residuals calculated by eq 4 were used to illustrate the range of the fit. The fits are not unique to each set of data; including polydispersity, for example, will give different predictions of the micellar length than if the system is considered monodisperse. However, the use of various models only highlights the physics that can be gained by the general form of the scattering data.

Figure 7 shows the scattered intensity $I(q)$ for 11 mM CTAT/11 mM NaCl/D_2O. The slope of $n = 1$ is indicated by the solid line. The general form of the data suggests the presence of rigid rods. Applying the model of rigid rods given in eqs 5 and 6 (with a calculated value for $\Delta\rho$ and R set equal to r_{cs} from Table 1) gives a micellar length of $L = 1500 \pm 200$ Å. To illustrate the range of the fit of this model, residuals showed slight overpredictions (up to 13%) at $0.002 < q < 0.01$ Å^{-1}. Note that the decision to shift the SLS data to match the SANS data (instead of vice versa) is arbitrary and only affect the terms given in eq 3 as scale and bkgd, not P(q). In Figure 8, the scattering from 11 mM CTAT/20 mM NaCl shows distinct deviation from $I \sim q^{-1}$ at low q, indicating flexible cylinders. Modeling with uniform flexible cylinders ($L = 1163 \pm 200$ Å and $L/b = 0.38 \pm 0.1$) begins to capture the "shoulder" in the scattering but drastically underpredicts the low-q scattering (up to 80%). Introducing polydispersity into the model yields the most satisfactory fit with $L = 835 \pm 120$ Å and $L/b = 0.9 \pm 0.2$. At 200 mM NaCl, the low-q shoulder is even more dramatic, as shown in Figure 9. Modeling with uniform flexible cylinders ($L = 2910 \pm 180$ Å, $L/b = 4.9 \pm 0.8$) gives underpredictions at $q < 0.01$ Å^{-1} that are similar to those observed for 20 mM NaCl. Including polydispersity in the model gives $L = 1558 \pm 230$ Å and $L/b = 2.9 \pm 0.7$ with smaller residuals throughout the range of q. At low NaCl concentrations, 0 and 2.2 mM NaCl, estimates for the micellar length and flexibility cannot be made because of the correlation (electrostatics) peak at $q \approx 0.012$ Å^{-1}. As described in the next section, rheological results can be used to estimate the micellar length for these unscreened systems if the micelles are assumed to be rigid. Values from the modeling of all other systems are reported in Table 2 for varying NaCl concentration.

4.3. Shear-Induced Structure. Under shear, anisotropic SANS scattering patterns emerge above a critical shear rate, indicating structural alignment in the direction of the flow. This anisotropy can be analyzed using an alignment factor, previously defined[16] as

$$A_f = \frac{I(q_{peak},\phi=\pi/2) - I(q_{peak},\phi=0)}{I(q_{peak},\phi=\pi/2)} \qquad (12)$$

For an isotropic system, A_f is 0, whereas for a fully aligned system, A_f approaches 1. This is a qualitative method that we invoked as a formalism for characterizing the anisotropic scattering patterns and extracting information about micellar alignment. Figure 10a shows A_f as a function of shear rate. At low shear rates, A_f is low. Above a critical shear rate, alignment increases dramatically for various CTAT/NaCl systems. In agreement with rheological measurements, only systems of 11 mM CTAT/D_2O with 0−4.4 mM NaCl form SIS. Although critical rates vary with composition of NaCl, the shifting critical behavior shown in Figure 10b indicates that there is a similarity in how all systems align: the transition is sharp,

Table 2. Effects of NaCl on Micellar Length and Flexibility

mol of NaCl: mol of CTAT	appropriate model[a]	$\Delta\rho$ (10^{10} cm^{-2})[e]	L (Å)	L/b	b (Å)
0:1	rheology-based[b]	6.13	470 ± 6	–	–
0.1:1	rheology-based	6.12	458 ± 10	–	–
0.2:1	rheology-based	6.12	444 ± 5	–	–
0.3:1	rheology-based	6.12	363 ± 6	–	–
0.4:1	rheology-based	6.12	362 ± 6	–	–
1:1	rigid cylinder[c]	6.12	1500 ± 200	–	–
1.8:1	polydisperse flexible cylinder[d]	6.11	835 ± 120	0.9 ± 0.2	987 ± 100
18:1	polydisperse flexible cylinder[d]	6.10	1558 ± 230	2.9 ± 0.7	547 ± 55

[a] See Results and Discussion sections for choice of appropriate model. [b] From Barentin and Liu.[15] [c] From Hayter and Penfold.[22] [d] From Pedersen and Schurtenberger.[23] [e] $\Delta\rho$ values are based on calculated values and are held constant for each NaCl concentration.

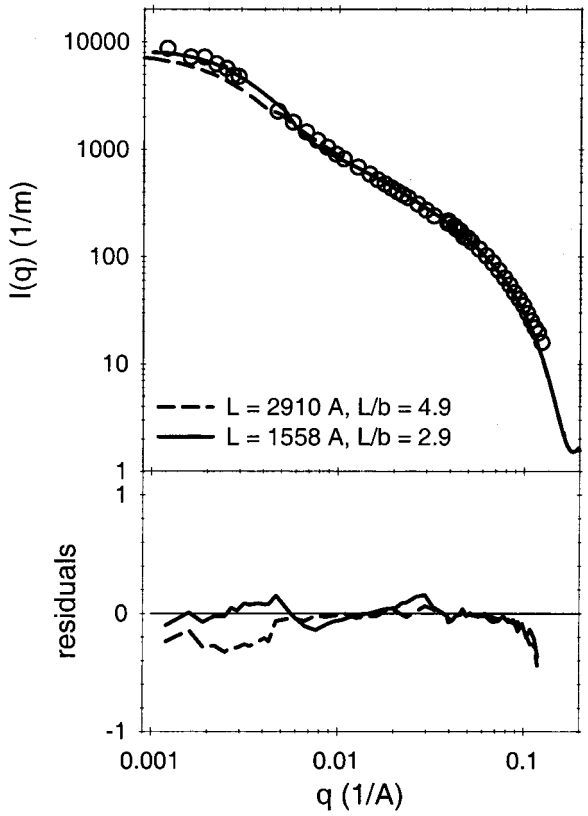

Figure 9. Comparison of various models for the scattering of 11 mM CTAT/200 mM NaCl in D_2O (18:1) (○). The dashed line (- - -) is the monodisperse flexible cylinder model, and the thick solid line (—) is the polydisperse, flexible cylinder model.[23] The best overall fit is given by polydisperse flexible cylinders.

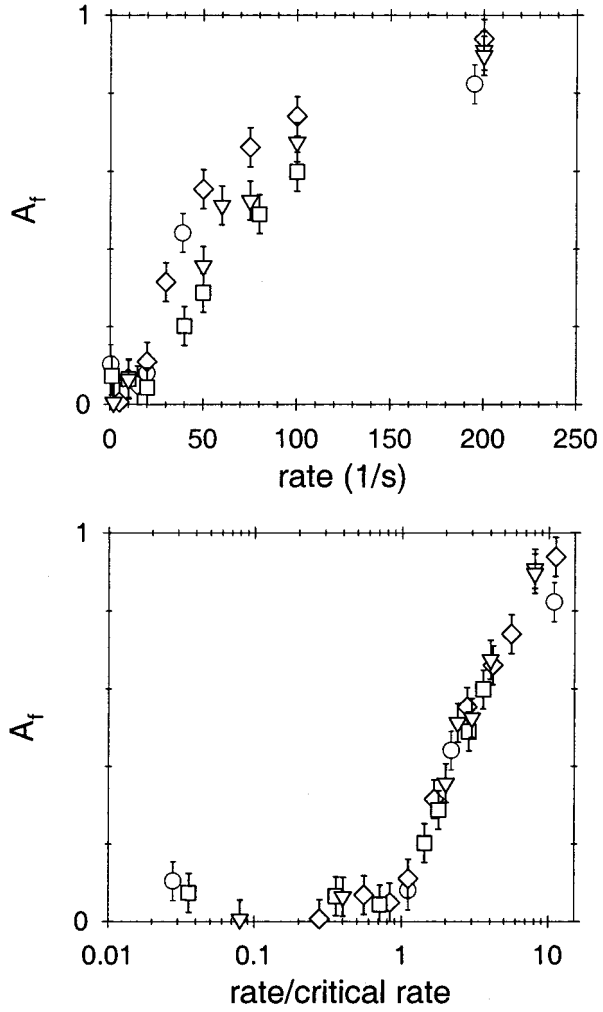

Figure 10. Effects of NaCl on the structural alignment of 11 mM CTAT at various molar ratios of NaCl to CTAT: (○) 0:1, (◇) 0.1:1, (□) 0.2:1, and (▽) 0.4:1. In the top figure the alignment factors, A_f, are shown as a function of the rate on a linear scale, whereas in the lower figure the horizontal axis is normalized by the critical shear rate for each individual NaCl/CTAT system and shown on a logarithmic scale.

with little or no alignment observed until the critical shear rate is reached. Beyond the critical rate, there is some universality in the steady-state level of alignment. This uniform behavior was seen in previous work, where a nonionic polymer was used to manipulate the critical shear rate of SIS formation.[16]

5. Discussion

The importance of significant electrostatic interactions in the formation of shear-induced structures (SIS) was confirmed: only systems that have a correlation peak in static scattering in the q range studied have apparent shear-thickening behavior in rheological studies and structural alignment in the shear SANS results (0−4.4 mM NaCl). At low concentrations, added NaCl increases the length of the micelles through screening electrostatic interactions, causing increases in η_o and decreases in the critical rates for shear thinning. Furthermore, shear SANS shows that there are similarities, i.e., universal behavior, in how all CTAT/NaCl systems align, even though the critical shear rates vary with NaCl concentration.

Barentin and Liu proposed a method of calculating the micellar length from the critical shear rates required for the formation of SIS in dilute systems of charged rodlike micelles.[15] Judging from rotational and translational motion, the critical shear rate was related to the micellar length (L), zero-shear viscosity (η_o), and Debye length (κ^{-1}). Implicit in this model is the assumption of rigid micelles. For systems of 11 mM CTAT/D_2O with 0−4.4 mM NaCl, this method was used to estimate L. For these calculations,

Debye lengths ranging from 4.4 to 11.4 nm were used on the basis of the NaCl concentration, the degree of Tos^- binding,[28] and the Debye−Huckel approximation. Values for L are reported in Table 2. Ranging from $L = 356-476$ Å, these values are comparable to the $L = 580$ Å value found for 9 mM CTAT/D_2O (a slightly lower concentration of CTAT than used in this work) by Berret et al.[7] According to this method, increasing the NaCl concentration does not increase micellar length, whereas the rheology, mainly the increases in η_o and decreases in critical rates for shear thinning (at low rates), strongly suggests the formation of longer micelles. This discrepancy comes from the inherent assumption of micellar rigidity in Barentin and Liu's model. Even though the model predicts the appropriate orders of magnitude of micellar lengths, it does not apply to these CTAT/NaCl systems because of the requirement of micellar rigidity. Unfortunately, the correlation peak in the scattering data does not allow for confirmation or denial of micellar rigidity at these low NaCl concentrations.

At higher NaCl concentrations, the rheology of the micellar systems changes dramatically. At 11 mM NaCl, electrostatic interactions are adequately screened, no SIS is formed, and the micelles are relatively rigid. At 20 mM NaCl, micelles become somewhat flexible, and a maximum in η_o and minimum in the critical rate required for shear thinning are obtained. At even higher NaCl concentrations (200 mM NaCl), the micelles are flexible, with $L/b = 2.9 \pm 0.7$, and there is a marked decrease in η_o. The degrees of flexibility found in this work for CTAT are similar to those of CTA/2,6-dichlorobenzoate found by Magid et al.[29] Increasing the NaCl concentration from 20 to 200 mM does not have a significant effect on the micellar length according to various models. It is obvious, however, that the main effect of NaCl is to increase the flexibility of the micelles at these higher NaCl concentrations. If one considers the micellar systems as being analogous to dilute polymer solutions, it is expected that a system of more rigid chains would have a higher η_o value than a system of more flexible chains of the same molecular weight (or contour length).[30] Furthermore, previous simulation work by Andrews and co-workers predicted that increasing the concentration of added salt in a polyelectrolyte system would increase the chain flexibility.[31] This change in the structure of the chain would lead to a decrease in η_o and an increase the critical shear rate required for shear thinning, as well as less dramatic shear thinning. As shown in Figures 1−3, making the analogy between polyelectrolytes and wormlike micelles shows that the increases in micellar flexibility are consistent with the rheology of these systems.

6. Conclusions

In this work, the effects of NaCl on the rheology and structure of CTAT micelles were investigated using rheological measurements and static light and neutron scattering methods. In particular, the influences of electrostatic interactions and micellar length and flexibility on the formation of shear-induced structures were investigated. Small amounts of electrolyte caused the growth of micelles by increasing the degree of screening electrostatic interactions, as shown by the increases in η_o and decreases in critical shear rates for shear-thinning behavior. The critical shear rates for SIS formation (apparent shear thickening) tend to increase with NaCl concentration for these systems. At salt concentrations greater than or equal to 11 mM NaCl, intermicellar electrostatic interactions are negligible, and no SIS is formed. At 11 mM NaCl, the micelles are somewhat rigid. At 20 mM NaCl, there is a maximum in η_o, and the micellar system exhibits a small degree of flexibility. Further increases in the salt concentration lead to more flexible micelles. This increased flexibility and resulting decrease in η_o and change in the shear-thinning behavior are consistent with expectations for dilute polymer and polyelectrolyte systems.

Acknowledgment. This work was made possible by funding from the National Science Foundation (NSF CTS-0092967 and NSF CTS-9871110) and the PPG Industries Foundation. SANS experiments were performed at NIST through funding from the NSF under Agreement DMR 9423101. The authors thank L. J. Magid, J.-F. Berret, and G. D. Patterson for constructive discussions.

LA015551X

(29) Magid, L. J.; Han, Z.; Li, Z.; Butler, P. D. *J. Phys. Chem. B* **2000**, *104*, 6717−6727.

(30) Doi, M.; Edwards, S. F. *The Theory of Polymer Dynamics*; Oxford University Press: New York, 1986.

(31) Andrews, N. C.; McHugh, A. J.; Schieber, J. D. *J. Polym. Sci. B: Polym. Phys.* **1998**, 1401−1417.